JOURNAL OF THERMOPHYSICS AND HEAT TRANSFER
Vol. 12, No. 1, January–March 1998

Detailed Heat Transfer Distributions Under an Array of Orthogonal Impinging Jets

Yizhe Huang,* Srinath V. Ekkad,† and Je-Chin Han‡
Texas A&M University, College Station, Texas 77843-3123

Detailed heat transfer distributions are presented for an array of in-line jets impinging orthogonally on a target plate with different crossflow orientations. A transient liquid crystal technique was used to measure the detailed heat transfer coefficients on the target surface. Different crossflow directions are created by changing the test section open ends. For each exit orientation, measurements are made at four flow Reynolds numbers between 4.8 × 10^3 and 1.83 × 10^4. Results show that the flow exit crossflow direction significantly affects the flow and heat transfer coefficient distributions on the target plate. Local heat transfer coefficient increases with an increase in average jet Reynolds number over the entire impingement target surface. Highest heat transfer coefficients are obtained for a crossflow orientation where flow exits in both directions. Nusselt number results are correlated for the various exit flow orientations.

Nomenclature

A = heat transfer surface area
d = impingement jet hole diameter
h = local convection heat transfer coefficient, W/m^2-K
k = thermal conductivity of acrylic material
k_{air} = thermal conductivity of air
$\dot{m}_c$ = crossflow mass flow rate, lbm/s
$\dot{m}_j$ = jet hole mass flow rate, lbm/s
Nu = Nusselt number, hd/k_{air}
P_a = ambient pressure
Pr = Prandtl number
P_1 = pressure in the pressure chamber
P_2 = pressure in the impingement channel
Re = average jet Reynolds number, $\rho Vd/\mu$
s = jet–jet spacing
T_i = initial temperature of test section
T_m = mainstream temperature of the flow
T_w = color change temperature of the liquid crystal, red-to-green
t = time of liquid crystal color change
V = average jet velocity
X = axial distance of the impingement surface
Y = spanwise distance of the impingement surface
Z = distance between jet plate and target plate
α = thermal diffusivity of acrylic material, and also jet inclination angle
μ = fluid dynamic viscosity
τ = time step

Introduction

JET impingement heat transfer has become well established as a high-performance technique for heating, cooling, or drying a surface. Impingement jet cooling systems have been used in advanced gas turbine engines, which operate at a high gas temperature (1300–1500°C) to improve thermal efficiency and power output. Gas turbine blades need to be cooled to operate under the allowable temperature condition without failure. Cooling by impinging jets on the heated interior surface of the turbine components is used in turbine blade internal cooling and combustion liner cooling.

There have been many experimental investigations and theoretical studies on the heat transfer characteristics of jet impingement. Chupp et al.[1] evaluated the internal heat transfer coefficient for impingement cooling on the leading edge of a turbine blade. Studies[2–7] summarized findings relating to parametric effects of geometry, temperature, crossflow, turbulence, etc., on jet impingement heat and mass transfer. Florschuetz et al.[5] determined the heat transfer characteristics for jet array impingement with the effect of an initial crossflow rate. They presented correlations for both in-line and staggered hole patterns, including effects of geometric parameters for one crossflow direction. Downs and James[8] presented a comprehensive literature survey of most jet impingement studies before 1987 and the correlations developed by those studies. Viskanta[9] reviewed the heat transfer characteristics of single and multiple isothermal turbulent air and flame jet impingement on the surface. Metzger and Bunker[10] and Bunker and Metzger[11] studied impingement cooling on turbine airfoil leading-edge regions with and without film coolant extraction. Huber and Viskanta[12,13] studied the effect of jet–jet spacing and compared heat transfer from target plate perimeter and center jet impingement in a confined, impinging array of axisymmetric air jets. All of the previously mentioned studies observed an increase in heat transfer with jet impingement. They presented the effects of various geometrical and flow parameters on jet impingement heat transfer. However, the effect of crossflow direction has not been investigated in the previous studies. The present study measures detailed heat transfer coefficient distributions under an array of impinging in-line jets under the effects of different crossflow orientations. The jet plate and impingement surface geometry have been maintained constant for all three crossflow orientations. Detailed heat transfer distributions are presented using a transient liquid crystal technique. Only Van Treuren et al.[14] have presented detailed distributions under impinging jets. They measured both local heat transfer coefficient and adiabatic wall temperature under the impinging jets. They used the Hue, saturation intensity (HSI) method for analyzing the liquid crystal color changes.

The present study employs a transient technique in conjunction with a thin thermochromic liquid crystal coating on the test surface. The liquid crystal technique in the present study

Received Aug. 29, 1996; revision received April 3, 1997; accepted for publication April 4, 1997.

*Mechanical Engineer, Turbine Heat Transfer Laboratory, Department of Mechanical Engineering; currently at Motorola, Inc., Austin, TX.

†Senior Project Engineer, Turbine Heat Transfer Laboratory, Department of Mechanical Engineering; currently at Allison Engine Company, Indianapolis, IN 46206-0420.

‡HTRI Professor, Turbine Heat Transfer Laboratory, Department of Mechanical Engineering. Associate Fellow AIAA.

is similar to the one presented by Ekkad and Han.[15] The thin coatings are sprayed directly on the impingement target surface and observed during a transient test with an automated computer vision and data acquisition system. The time of color change of the liquid crystals to green is measured using an image processing unit. The high resolution of the technique will provide a detailed understanding of the jet impingement cooling process. This transient technique using liquid crystals is well established and can be applied to complex geometry, as well as provide a high resolution that cannot be achieved using multiple thermocouples. The detailed results will also help in validation of computational methods to model jet impingement flows.

Test Description and Apparatus

Reorientation of the crystal lattice displays liquid crystal color with different wavelengths of light reflected, depending on the coating temperature. The time of color change of the liquid crystals during a transient test is measured using a red, green, blue (RGB) camera and a computer vision system.

Figure 1 shows the entire test setup. The computer vision data acquisition system consists of an RGB camera to view the liquid-crystal-coated test surface during the thermal transient test. The composite color signal is split into red, green, and blue colors and is passed on to the color frame grabber board in the personal computer. The frame grabber board is programmed to analyze the color change using image processing software. The picture can be adjusted using a video monitor as a reference. The software analyzes the picture frame-by-frame for color changes. The analysis records the time of transition of the liquid crystals from colorless to green at each point on the test surface during the transient test.

Figure 2 shows the three-dimensional schematic diagram of the test section. It consists of two compartments joined by an orifice plate, which has an array of jet holes with diameters of 0.635 cm. The jet orifice plate thickness is equal to the jet hole diameter. There are 12 rows of 4 holes, and a total of 48 holes on the orifice plate. The jet-to-jet spacing is 4 hole diameters. The length of the test section is 30.48 cm. The inlet pressure chamber has a cross-sectional area of 10.16 $\times$ 2.54 cm, and the impingement channel has a cross-sectional area of 10.16 $\times$ 1.905 cm. The distance between the jet orifice plate and the impingement target surface is three times the jet hole diameter. The jet plate geometry was chosen to be a typical case based on results from other studies. Since the focus of this paper is on the effect of crossflow orientation, a typical jet plate geometry was chosen for representation. The perforations in the jet plate result in a series of jet flows when a pressure difference is applied across the orifice plate. The test section is made of clear acrylic material. The impingement target surface is made from black acrylic sprayed with liquid crystals on the inside surface. The thickness of the test plate is 0.508 cm. A camera observes the test surface through the transparent walls (Fig. 1).

Figure 3 shows the schematic of a series of jets in the impingement test section. The three flow orientations are obtained by changing the discharge openings. Note that the top chamber is the pressure chamber and the bottom chamber is the impingement channel. There is a 91.44-cm plenum chamber through which the flow develops before entering the pressure chamber. The three orientations provide different crossflow effects created by the spent jets exiting out of the impingement channel. The three exit flow orientations are studied to determine which orientation provides the better impingement cooling effect.

The test section connects to a compressor-based air supply with a standard orifice meter measuring the airflow rate. The airflow is controlled to the required flow rate and heated to a preset temperature using an in-line air heater. A three-way ball diverter valve routes the air away from the test rig when no test is in progress. A strip chart recorder measures the mainstream flow temperature from a thermocouple during the transient test (Fig. 1).

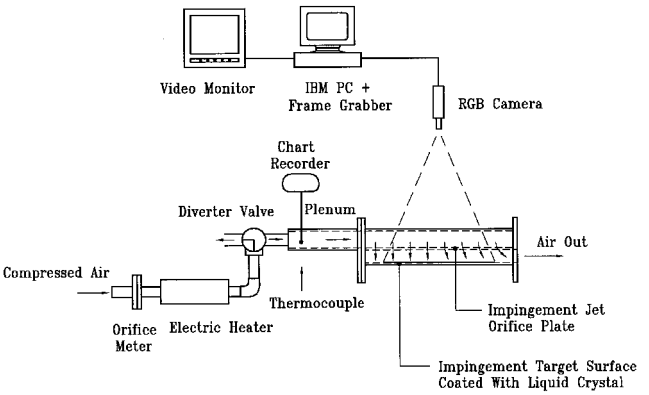

Fig. 1 Schematic of the experimental setup.

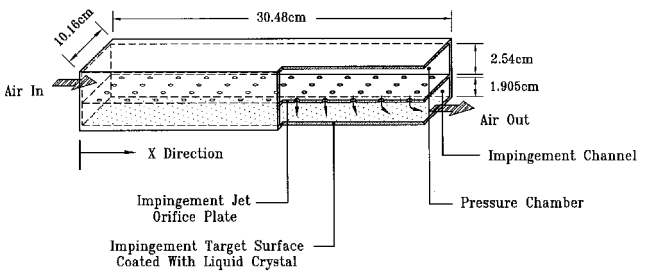

Fig. 2 Schematic of the test section for flow orientation 1.

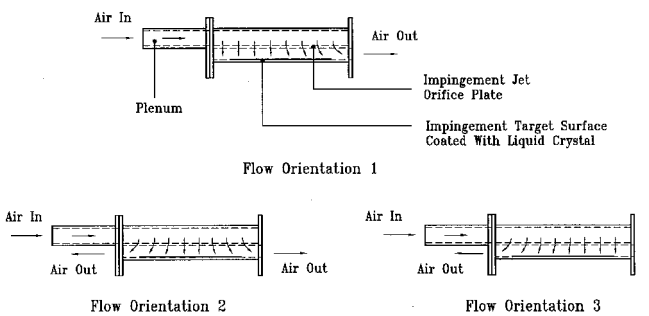

Fig. 3 Illustration of the three exit flow orientations.

Pressure taps are instrumented into the test section at various locations in the pressure and impingement channels to measure the pressure drop across the jet plate. The measured pressure drop values are used to calculate the mass flow rate through jet holes and the amount of crossflow in the impingement channel.

Procedure

The test section is assembled after spraying the liquid crystals. The camera is set up and focused on the coated surface. Each test run is a thermal transient, initiated by the sudden introduction of heated air to the test section, which results in a color change of the surface coating. A test run begins with heated air diverted away from the test section so that the test channel walls remain at the laboratory ambient temperature. The valve remains in the diverted position until steady flow and a preset temperature (65–45°C for $Re = 4.85 \times 10^3$–1.83×10^4) have been achieved in the diversion flow loop. Then, the valve is switched to route the hot air into the test section, and the computer data acquisition program and the chart recorder are simultaneously switched on to measure time and temperature data. The data acquisition system records the transition time for the color change to green (32.7°C), and transfers the data into a matrix of time of the color change over the

entire surface. The time and temperature data are entered into a computer program to obtain the local heat transfer coefficient. The average uncertainty in heat transfer coefficient measurement, estimated by the method of Kline and McClintock,[16] is about ±5.9%. The individual uncertainties in the measurement of the time of color change ($\Delta t = \pm 0.5$ s), the mainstream temperature ($\Delta T_m = \pm 1$°C), the color change temperature ($\Delta T_w = \pm 0.2$°C), and the wall material properties ($\Delta\alpha/k^2 = \pm 5\%$). These uncertainties were included in the calculation of the overall uncertainty in the measurement of h.

Heat Transfer Theory

A one-dimensional transient conduction model into a semi-infinite surface with a convective boundary condition at the surface is assumed.[15] The surface temperature response is described by the following solution:

$$\frac{T_w - T_i}{T_m - T_i} = 1 - \exp\left(\frac{h^2\alpha t}{k^2}\right) \operatorname{erfc}\left(\frac{h\sqrt{\alpha t}}{k}\right) \tag{1}$$

The coefficient h can be calculated from Eq. (1), by knowing the initial temperature ($T_i \approx 27$°C) of the test surface and the mainstream temperature ($T_m \approx 50$°C), and measuring the color change time t for the liquid crystal coated surface to reach color change temperature ($T_w \approx 32.7$°C). The duration of the testing time is kept small so that the semi-infinite solid assumption is valid for the test plate of 0.508 cm thickness. The mainstream is heated to a temperature that produces color change times from 10–60 s. The testing time is much shorter than the time required for the temperature to penetrate the acrylic material. The chart recorder measures the gradual change of the mainstream temperature during the transient test. Figure 4 presents a typical mainstream temperature variation with time during the transient test. The mainstream temperature is measured at the inlet of the pressure channel. The heat transfer coefficients calculated on the impingement surface are based on this measured temperature. The chart recorder output is the spline curve. The mainstream temperature cannot be represented as a single step change. Since the mainstream temperature now depends on time, the solution must include the gradual change of the temperature. The time history of the mainstream temperature is reproduced as a series of step functions as shown in Fig. 4. Using the Duhamel's superposition theorem, the solution in Eq. (1) is represented as

$$T_w - T_i = \sum_{j=1}^{N} \left[1 - \exp\left(\frac{h^2\alpha(t-\tau_j)}{k^2}\right) \times \operatorname{erfc}\left(\frac{h\sqrt{\alpha(t-\tau_j)}}{k}\right)\right] [\Delta T_{mj}] \tag{2}$$

where ΔT_m and τ_j are the temperature and time step changes from the chart recorder output. Equation (2) is solved to obtain the local heat transfer coefficient at every point on the measured region (250 × 100 points). The average Nusselt number variation with Reynolds number for all three flow orientations compared with the multiple jet heat transfer correlations[2,5,15] will be presented.

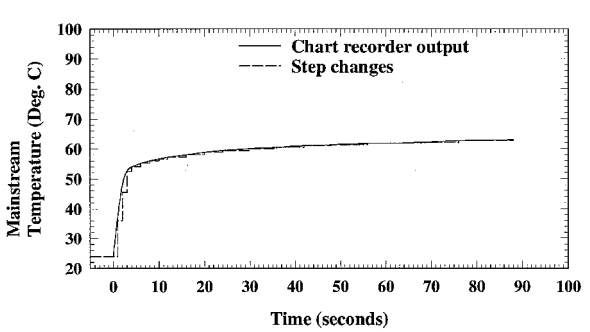

Fig. 4 Typical mainstream temperature distribution during transient test.

Results and Discussion

Jet impingement heat transfer is dependent on several flow and geometrical parameters. The jet impingement Nusselt number is presented as a functional form of these parameters:

$$Nu = (hd/k_{\text{air}}) = f[Re, Pr, (X/d, Y/d, Z/d, \alpha), \text{flow orientation, surface geometry, jet inlet condition . . .}] \tag{3}$$

where Re and Pr are the flow parameters. The jet spacing to diameter ratio (X/d, Y/d), jet plate to target plate distance to diameter ratio (Z/d), and the jet inclination angle α are the geometric parameters. The flow exit direction and the target surface geometry are also important parameters having a significant effect on impingement heat transfer. The jet inlet condition is the direction in which the flow enters the pressure channel.

Flow Distributions

The local pressure distributions are measured by placing static pressure taps inside the test section. Static pressure was measured at each location for each Reynolds number and flow orientation. The static pressure differences between the pressure chamber and the impingement channel, and also the ambient, help determine the impingement and crossflow mass flow rates. The heat transfer distributions have to be consistent with the static pressure distributions to obtain a better understanding of the flow through the impingement channel. The tests are performed at four average jet Reynolds numbers of 4.85×10^3, 9.55×10^3, 1.28×10^4, and 1.83×10^4 for all three flow orientations.

The X location starts from the supply end of the channel. For the exit flow orientation 1, flow enters at $X/d = 0$ and exits at $X/d = 48$. For exit flow orientation 2, flow exits from both ends ($X/d = 0$ and $X/d = 48$), and the flow exits at $X/d = 0$ for orientation 3. Figure 5a presents the mass flow rate through each of the 12 rows of holes for each exit flow orientation. The jet flow distribution through each row is presented here for $Re = 1.83 \times 10^4$. Because the flow enters the pressure channel from one end of the channel, it is imperative that there be a slightly uneven distribution of flow through each jet row. However, from the figure, it is evident that the entrance effect is small. It appears that the jet flow rate increases with increas-

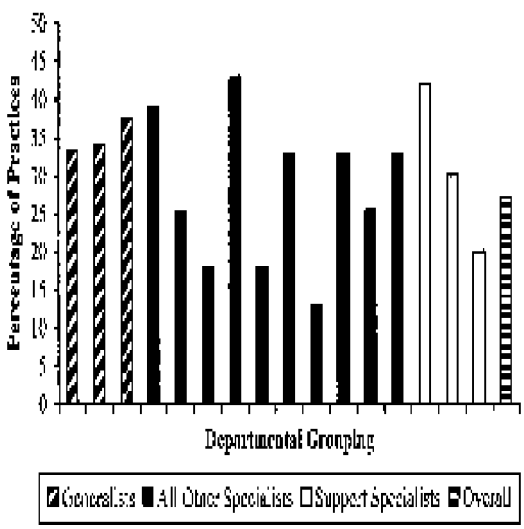

Fig. 5 Jet flow rate and crossflow rate distributions for the three exit flow orientations.

ing X/d for flow orientations 1 and 2. More jet exits out of the holes with least resistance. In the case of orientation 3, the jets appear to exit more toward the exit opening end at low X/d.

Figure 5b presents the mass flow ratio of crossflow-to-total jet flow for all three exit flow orientations. For orientation 1, crossflow develops at low X/d and increases toward the exit. At large X/d, nearly 80% of the total flow exits the test section as crossflow. This is typical of that seen by Florschuetz et al.[5] Florschuetz et al.[5] also studied a crossflow that is similar to that of flow orientation 1 from the present study. For flow orientation 2, there is a stagnation point in the middle of the target plate where the crossflow develops toward both ends of the test section. However, the stagnation location is not in the middle of the test section, which causes more crossflow toward the opening at large X/d. For flow orientation 3, crossflow develops at large X/d and increases toward the exit at X/d = 0. The heat transfer distributions are significantly affected by the crossflow development and direction.

Detailed Local Heat Transfer Coefficients

Figures 6–8 show detailed local Nusselt number distributions for the three flow orientations as the function of nondimensional location Y/d and X/d on the test surface for all four Reynolds numbers. The results are presented from X/d = 3.5 to X/d = 44.5 in the streamwise or axial direction over the entire span, where X is defined from the supply side of the test section. The hole locations are indicated on the detailed distributions for each case. Results are shown for the 10 middle rows; measurements were not taken for the jet rows near the ends of the plate.

Figure 6 presents the detailed distributions for flow orientation 1. Results show an increase in the local Nusselt number for an increase in jet Reynolds number. For this flow orientation, the flow enters the pressure chamber from one direction (X/d = 0) and exits the impingement channel in the same direction on the opposite end (X/d = 48). The heat transfer coefficient decreases as X/d increases. From Fig. 5b it is evident that the crossflow increases with increasing X/d. The jets show strong impingement at small X/d, where the crossflow is very weak. Further downstream, the jets are pushed away from the target surface because of a stronger crossflow. This reduces the jet impingement, thus decreasing the local heat transfer coefficient underneath the jets. Also, the jets appear to show a shift in impingement location at large X/d because of the crossflow effect.

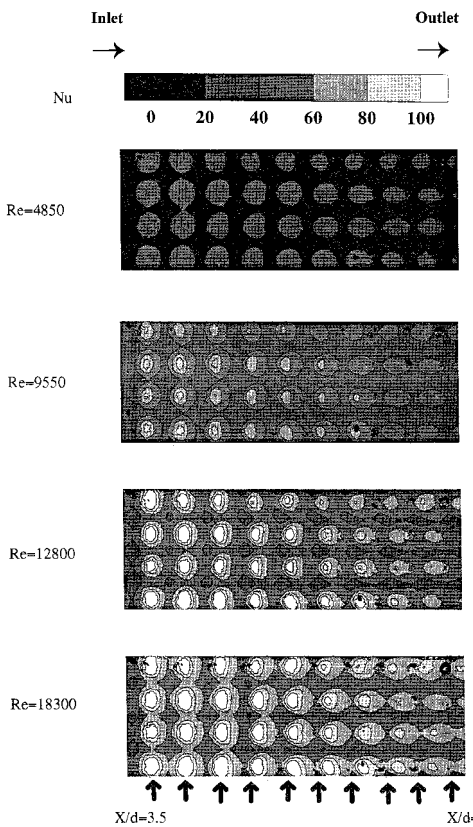

Fig. 6 Detailed Nusselt number distributions for exit flow orientation 1.

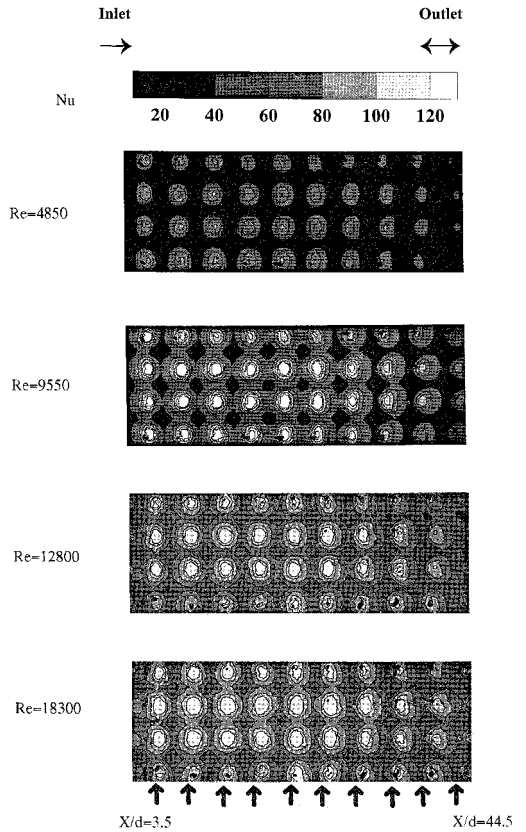

Fig. 7 Detailed Nusselt number distributions for exit flow orientation 2.

Figure 7 presents the detailed distributions for flow orientation 2. In this case, the flow exits in both directions. The highest heat transfer coefficients are under the jets near the center of the test plate. The heat transfer coefficients decrease toward the exit ends with the development of crossflow. As seen from Fig. 5b, the heat transfer coefficients are highest around X/d = 22, where the crossflow is minimum. Crossflow is stronger at large X/d, causing lower heat transfer coefficients than at small X/d.

Figure 8 presents the detailed distributions for flow orientation 3. In this case, the flow exits at the supply end of the test section. The detailed Nusselt number distributions show that the crossflow reduces local heat transfer coefficients under the jets at small X/d. Jet impingement is stronger at large X/d, where crossflow is minimum. However, it can be noted that the highest heat transfer coefficient underneath the jets at large X/d is lower than that for the other two cases in regions with minimum crossflow. This may be because more flow exits at holes near the exit. Lower mass flow rate through holes at large X/d produces lower heat transfer coefficients. A shift in the jet impingement location occurs at small X/d because of the increased crossflow effect.

The effect of jet Reynolds number for flow orientations 2 and 3 is similar to that for flow orientation 1. An increase in Reynolds number increases local heat transfer coefficients over the entire target surface.

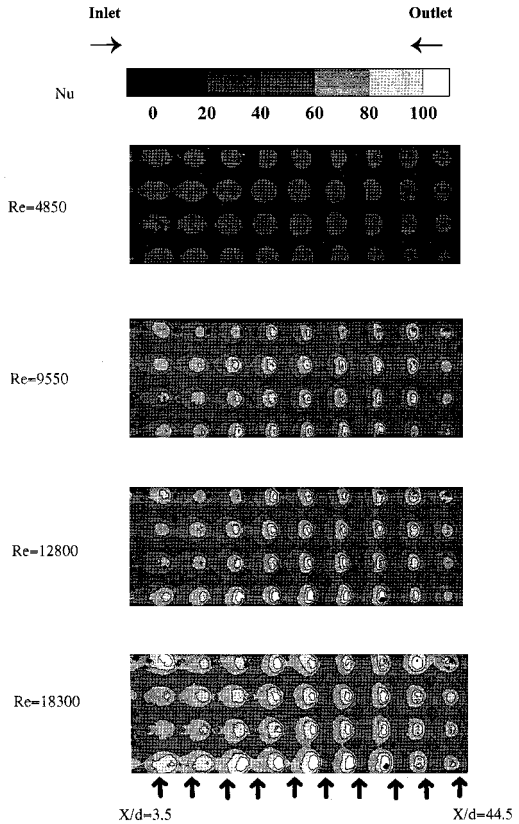

Fig. 8 Detailed Nusselt number distributions for exit flow orientation 3.

Span-Averaged Nusselt Number Distributions

Figure 9 shows the effect of Reynolds number on span-averaged Nusselt number distributions for three flow orientations. The arrows along the nondimensional axial location X/d indicate the locations of the 12 rows of impingement jets. However, results are presented only for the middle 10 rows. The entrance and exit flow directions are shown for each flow orientation. Note that the Nusselt numbers increase with an increase in Reynolds number for all three flow orientations over the entire channel. For flow orientation 1, the Nusselt numbers decrease toward the exit direction (large X/d). The effect of crossflow reduces the Nusselt number at large X/d. The jets also appear to tilt toward the crossflow direction for large X/d. For flow orientation 2, the crossflow appears to have an effect only on the two end jets on both sides. Since crossflow is in both directions in this case, the Nusselt numbers at small and large X/d are both lower than that in the middle of the channel. For flow orientation 3, the crossflow reduces the Nusselt number at small X/d. In this case, the jets at large X/d away from the channel exit also produce low Nusselt numbers because of decreased jet velocities. Although jet velocities increase near the exit, the Nusselt numbers are lower because of the crossflow effect that decreases the impingement effect of the jets at low X/d.

Figure 10 presents the effect of flow orientation on the span-averaged Nusselt numbers for $Re = 9.55 \times 10^3$. Flow orientation 2 provides the highest heat transfer coefficients over the entire surface, while flow orientation 3 provides the lowest. The crossflow has a limited effect for flow orientation 2 compared to that for orientations 1 and 3. The Nusselt numbers for flow orientation 3 might be lower because of the exit of the impingement channel being on the same side as the inlet to the pressure chamber. The tilt in the direction of the Nusselt number distributions under the jet clearly indicates the crossflow direction for flow orientations 1 and 3. Flow orientation 2 provides the highest impingement heat transfer performance at all jet Reynolds numbers.

Prior studies on jet impingement have involved studying the effects of several geometrical and flow parameters to develop a correlation for the heat transfer coefficient under jet impingement. Correlations by Kercher and Tabakoff,[2] Florschuetz et al.,[5] and Van Treuren et al.[14] are compared to the averaged results from the present study (Fig. 11). Kercher and Tabakoff's investigation[2] involved a crossflow effect that is similar to that of orientation 1 from the present study. They varied the number of jets, the jet hole diameter, the hole spacing in x, y

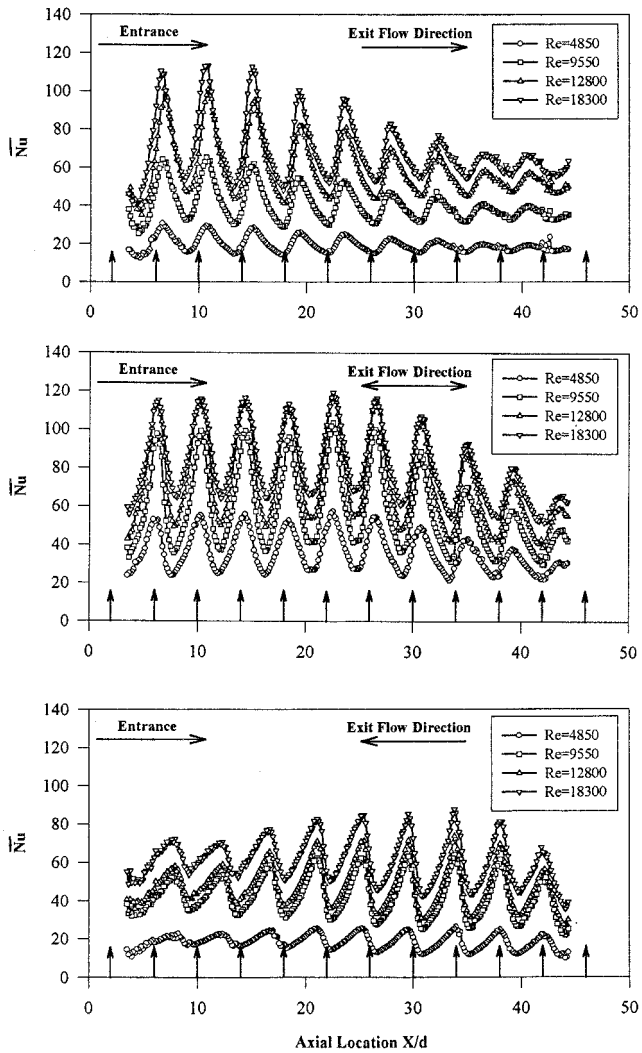

Fig. 9 Effect of Reynolds number on span-averaged Nusselt number for the three exit flow orientations.

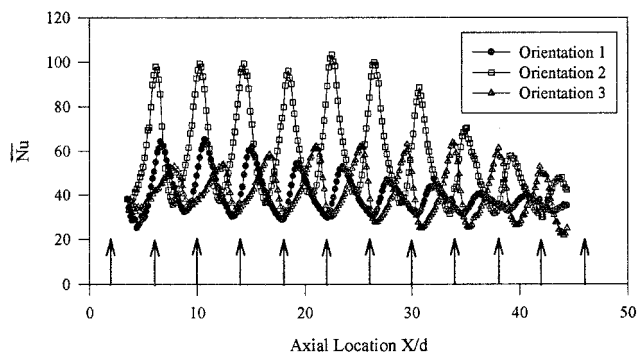

Fig. 10 Effect of exit flow orientation on span-averaged Nusselt number for $Re = 9.55 \times 10^3$.

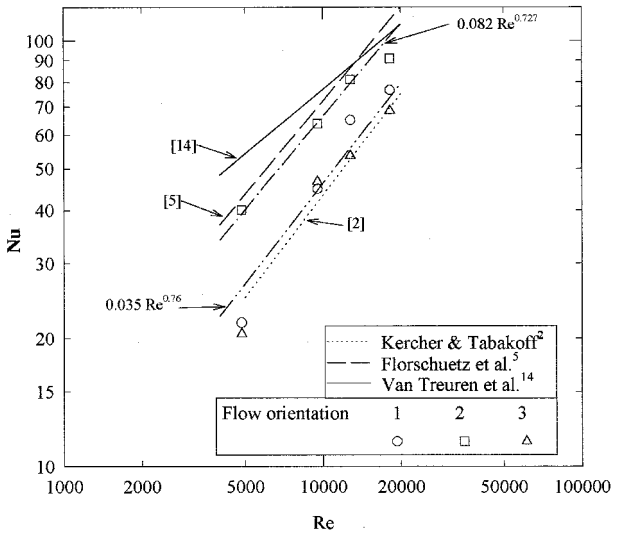

Fig. 11 Overall-averaged Nusselt number comparisons with existing multiple jet correlations.

direction ($X/d = Y/d$), and the jet plate to target plate distance. Based on all of these geometrical parameters, they proposed a correlation of the form $Nu = \phi_1\phi_2 Re^m (z/d)^{0.91} Pr^{1/3}$, where ϕ_1 and ϕ_2 are constants based on X/d and Y/d, respectively. Florschuetz et al.[5] presented correlations with different coefficients for in-line and staggered rows. They presented a correlation that is jet impingement for minimum crossflow, and also a correlation for developing crossflow. The correlation for jet impingement with minimum crossflow is given as $Nu = 0.363(X/d)^{-0.554}(Y/d)^{-0.422}(Z/d)^{0.068} Re_j^{0.727} Pr^{1/3}$. Van Treuren et al.[14] correlated their Nusselt number underneath the jet for Reynolds number dependence. They studied the effect of jet plate to target plate distance. Their hole spacing was eight hole diameters in the X and Y directions. They studied both in-line and staggered arrays. Their correlation for Nusselt number underneath the jets was $Nu = 0.685 Re^{0.496}$.

The detailed results from the present study are averaged over the entire target plate to produce a single averaged Nusselt number. The averaged Nusselt numbers for each orientation are plotted against the Reynolds number. The present results for the orientations 1 and 3 correlate for Reynolds number dependence as $Nu = 0.035 Re^{0.76}$. The correlation of Kercher and Tabakoff[2] is in good comparison with the results for orientations 1 and 3. Kercher and Tabakoff[2] presented results for crossflow effect similar to that for flow orientation 1. The correlation from Florschuetz et al.[5] is for the case with minimum crossflow. The results are higher than the present study results, which include the effects of crossflow. Similarly, the results for Van Treuren et al.[14] are also for the jet stagnation Nusselt numbers, which are higher than the averaged Nusselt numbers from the present study. The results for orientation 2 correlate with the Reynolds number as $Nu = 0.082 Re^{0.727}$. This correlation is in good agreement with the correlation of Florschuetz et al.[5] From the results, it is evident that the crossflow has a stronger effect for orientations 1 and 3, compared to orientation 2.

Conclusions

The effect of exit flow orientations on local heat transfer coefficients for multiple jet impingement under four jet Reynolds numbers is investigated. The conclusions are as follows.

1) Detailed heat transfer coefficient distributions are measured using a transient liquid crystal technique. The detailed distributions provide a better understanding of the heat transfer enhancement by impinging jets on a surface, and they also provide a reference for computational fluid dynamics-based studies relating to jet impingement heat transfer. The effect of crossflow orientation was studied for various jet Reynolds numbers.

2) The local Nusselt number on the entire impingement surface is dependent on the average jet Reynolds number. The local Nusselt numbers increase with an increase in jet Reynolds numbers.

3) The heat transfer coefficient distributions are significantly affected by crossflow direction. A crossflow direction where the flow exits both sides of the chamber provides the highest Nusselt numbers on the surface. Jet impingement is least affected by oncoming crossflow compared to the other two cases.

4) Overall average Nusselt numbers are correlated with Reynolds number dependence. Results compare well with published correlations. Overall averaged Nusselt numbers can be correlated together for crossflow orientations with only one side open. However, the Nusselt numbers for crossflow orientation with both sides open is represented by a different correlation.

Acknowledgment

The Texas Higher Education Coordinating Board—Advanced Technology Program supported this project under Grant 999903-165 (TEES 32190-71720ME).

References

[1]Chupp, R. E., Helms, H. E., McFadden, P. W., and Brown, T. R., "Evaluation of Internal Heat Transfer Coefficients for Impingement Cooled Turbine Blades," *Journal of Aircraft*, Vol. 6, No. 1, 1969, pp. 203–208; also AIAA Paper 68-564, 1968.

[2]Kercher, D. M., and Tabakoff, W., "Heat Transfer by a Square Array of Round Air Jets Impinging Perpendicular to a Flat Surface Including the Effect of Spent Air," *Journal of Engineering and Power*, Vol. 92, No. 1, 1970, pp. 73–82.

[3]Chance, J. L., "Experimental Investigation of Air Impingement Heat Transfer Under an Array of Round Jets," *TAPPI*, Vol. 57, No. 1, 1974, pp. 108–112.

[4]Florschuetz, L. W., Berry, R. A., and Metzger, D. E., "Periodic Streamwise Variation of Heat Transfer Coefficients for Inline and Staggered Arrays of Circular Jets with Crossflow of Spent Air," *Journal of Heat Transfer*, Vol. 102, No. 1, 1980, pp. 132–137.

[5]Florschuetz, L. W., Truman, C. R., and Metzger, D. E., "Streamwise Flow and Heat Transfer Distribution for Jet Impingement with Crossflow," *Journal of Heat Transfer*, Vol. 103, No. 2, 1981, pp. 337–342.

[6]Obot, N., and Trabold, T. A., "Impingement Heat Transfer Within Arrays of Circular Jets. Part I: Effects of Minimum, Intermediate, and Complete Crossflow for Small and Large Spacings," *Journal of Heat Transfer*, Vol. 109, No. 4, 1987, pp. 872–879.

[7]Florschuetz, L. W., Metzger, D. E., Su, C. C., Isoda, Y., and Tseng, H. H., "Heat Transfer Characteristics for Jet Array Impingement with Initial Crossflow," *Journal of Heat Transfer*, Vol. 106, No. 1, 1984, pp. 34–41.

[8]Downs, S. J., and James, E. H., "Jet Impingement Heat Transfer—A Literature Survey," American Society of Automotive Engineers, Paper 87-HT-35, 1987.

[9]Viskanta, R., "Heat Transfer to Impinging Isothermal Gas and Flame Jets," *Experimental Thermal and Fluid Science*, Vol. 6, No. 1, 1993, pp. 113–134.

[10]Metzger, D. E., and Bunker, R. S., "Local Heat Transfer in Internally Cooled Turbine Airfoil Leading Edge Regions: Part I—Impingement Cooling Without Film Coolant Extraction," *Journal of Turbomachinery*, Vol. 112, No. 3, 1990, pp. 451–458.

[11]Bunker, R. S., and Metzger, D. E., "Local Heat Transfer in Internally Cooled Turbine Airfoil Leading Edge Regions: Part II—Impingement Cooling with Film Coolant Extraction," *Journal of Turbomachinery*, Vol. 112, No. 3, 1990, pp. 459–466.

[12]Huber, A. M., and Viskanta, R., "Comparison of Convective Heat Transfer to Perimeter and Center Jet in a Confined, Impinging Array of Axisymmetric Air Jets," *International Journal of Heat and Mass Transfer*, Vol. 37, No. 10, 1994, pp. 3025–3030.

[13]Huber, A. M., and Viskanta, R., "Effect of Jet-Jet Spacing on

Convective Heat Transfer to Confined, Impinging Arrays of Axisymmetric Air Jets,'' *International Journal of Heat and Mass Transfer*, Vol. 37, No. 10, 1994, pp. 2859–2869.

[14]Van Treuren, K. W., Wang, Z., Ireland, P. T., and Jones, T. V., ''Detailed Measurements of Local Heat Transfer Coefficient and Adiabatic Wall Temperature Beneath an Array of Impingement Jets,'' *Journal of Turbomachinery*, Vol. 116, No. 2, 1994, pp. 369–374.

[15]Ekkad, S. V., and Han, J. C., ''Local Heat Transfer Distributions Near a Sharp 180° Turn of a Two-Pass Smooth Square Channel Using a Transient Liquid Crystal Image Technique,'' *Journal of Flow Visualization and Image Processing*, Vol. 2, No. 3, 1995, pp. 285–297.

[16]Kline, S. J., and McClintock, F. A., ''Describing Uncertainties in Single Sample Experiments,'' *Mechanical Engineering*, Vol. 75, No. 1, 1953, pp. 3–8.